# A Novel Neural Network Computing Based Way to Sensor and Method Fusion in Harsh Operational Environments

Yuriy V. Shkvarko, Juan I. Yañez and Gustavo D. Martín del Campo

Department of Electrical Engineering, Center for Advanced Research and Education of the National Polytechnic Institute, CINVESTAV-IPN, Guadalajara, Mexico

**Abstract.** We address a novel neural network computing-based approach to the problem of near real-time feature enhanced fusion of remote sensing (RS) imagery acquired in harsh sensing environments. The novel proposition consists in adapting the Hopfield-type maximum entropy neural network (MENN) computational framework to solving the RS image fusion inverse problem. The feature enhanced fusion is performed via aggregating the descriptive experiment design with the variational analysis (VA) inspired regularization frameworks that lead to an adaptive procedure for proper adjustments of the MENN synaptic weights and bias inputs. We feature on the considerably speeded-up implementation of the MENN-based RS image fusion and verify the overall image enhancement efficiency via computer simulations with real-world RS imagery.

## 1 Introduction

**Relation to Prior Work**–Demanding requirements of feature enhanced remote sensing (RS) imaging in harsh sensing environments has spurred development of various sensor/method fusion techniques for feature enhanced recovery of images acquired with multimode RS systems, e.g., see [1–16] and the references therein. The crucial problem is to reduce the fusion complexity and attain the (near) real-time processing mode. In this study, we propose a novel approach for computationally speeded-up enhancement of the RS imagery via adapting the Hopfield-type maximum entropy neural network (MENN) computational framework to solving the RS image fusion inverse problem. The feature enhanced fusion is performed via aggregating the descriptive experiment design with the variational analysis (VA) inspired regularization frameworks that lead to an adaptive procedure for proper adjustments of the MENN synaptic weights and bias inputs. Our MENN image enhancement technique outperforms the recently proposed competing methods (e.g., the F-SAR-adapted anisotropic diffusion (AD) method [13], the maximum likelihood (ML) inspired amplitude-phase estimator (APES) [15], the robust spatial filtering (RSF) and robust adaptive spatial filtering (RASF) procedures [16, 17], etc. that do not employ the method fusion). We feature on the considerably speeded-up implementation of the MENN-based RS image fusion and verify the overall image enhancement efficiency via computer simulations with real-world RS imagery.

Shkvarko Y., Yañez J. and Martín del Campo G..
A Novel Neural Network Computing Based Way to Sensor and Method Fusion in Harsh Operational Environments.
DOI: 10.5220/0005125100190026
In *Proceedings of the International Workshop on Artificial Neural Networks and Intelligent Information Processing* (ANNIIP-2014), pages 19-26
ISBN: 978-989-758-041-3

## 2 Problem Model

In RS imaging, a model most often used expresses the degraded lexicographically ordered image vector formed by a system as a sum of the noise and a linear convolution of the original scene image with the system spatial response function. The latter is usually referred to as the point-spread function (PSF) of the RS image formation system [1–8]. The noise vector is account to the power components in the degraded image that correspond to system noise and environmental noise (solution-dependent in the harsh environments due to multiplicative noise effects [8]). Let us consider for the purpose of generality $P$ different degraded images $\{\mathbf{g}^{(p)}; p = 1, \ldots, P\}$ of the same original scene image $\mathbf{b}$ obtained with $P$ different RS imaging systems or methods.

The system or method fusion paradigm [11, 12] can be employed in these cases to improve the image quality. In a system fusion context [11], we associate $P$ different models of the PSF with the corresponding image formation RS systems. In the method fusion context [12], we assume one given low resolution image acquisition system but apply $P$ different image formation algorithms to form the images $\{\mathbf{g}^{(p)}; p = 1, \ldots, P\}$, e.g., from the DEDR or VA families developed in the previous studies [13–17]. In the both cases, the lexicographically ordered [5, 12] $K$-D low resolution RS image model is formalized by a system of $P$ equations

$$\mathbf{g}^{(p)} = \mathbf{\Phi}^{(p)}\mathbf{b} + \mathbf{v}^{(p)}; \qquad p = 1,\ldots, P \tag{1}$$

with $P$ different $K \times K$ PSFs $\mathbf{\Phi}^{(p)}$ and related K-$D$ noise vectors $\{\mathbf{v}^{(p)}\}$, respectively. The problem of image enhancement is considered as a composite inverse problem of restoration of the original $K$-D image $\mathbf{b}$ from $P$ actually formed degraded $K$-D RS images $\{\mathbf{g}^{(p)}\}$, given the systems' PSFs $\{\mathbf{\Phi}^{(p)}\}$. No prior knowledge about the statistics of noise $\{\mathbf{v}^{(p)}\}$ in the data (1) is implied, thus the maximum entropy (ME) prior model uncertainty [11, 12] conventional for harsh sensing environments is assumed.

## 3 ME Regularization

It is well known that the PSFs $\{\mathbf{\Phi}^{(p)}\}$ are ill-conditioned for practical low/medium resolution RS image formation systems, both passive radiometers and active radar/fractional SAR sensors [1–8]. Hence, the regularization-based approach is needed when dealing with the feature enhanced RS image recovery problems. Next, the statistical model uncertainties about the image and noise significantly complicate the recovery problem making inapplicable the statistically optimal Bayesian inference techniques [5]. That is why, we adopt here the ME regularization approach [11, 12, 16, 17] in which case the desired feature enhanced RS image is to be found as a solution $\hat{\mathbf{b}} = \arg\min_{\mathbf{b}} E\left(\mathbf{b}|\boldsymbol{\lambda}\right)$ to the problem of minimization of the augmented objective/cost function

$$E(\mathbf{b} \mid \boldsymbol{\lambda}) = -H(\mathbf{b}) + \tfrac{1}{2}\sum_{p=1}^{P}(\lambda_p J_p(\mathbf{b})) + \tfrac{1}{2}\lambda_{P+1}J_{P+1}(\mathbf{b}) \tag{2}$$

where $H(\mathrm{b}) = -\sum_{k=1}^{K} b_k \ln b_k$ is the image entropy, $\boldsymbol{\lambda} = (\lambda_1, \ldots, \lambda_P, \lambda_{P+1})^{\mathrm{T}}$ is the vector of regularization parameters, $\{J_p(\mathbf{b}); p = 1, \ldots, P\}$ compose a set of objective (cost) functions incorporated into the optimization; here, we compose $\{J_p(\mathbf{b}); p = 1, \ldots, P\}$ of equibalanced image discrepancy and image gradient map discrepancy $\ell_2$ structured squared norms instead of only image discrepancy terms considered in the previous competing studies [12–15]. Also, the second novel proposition of this study consists in constructing $J_{P+1}(\mathbf{b}) = \mathbf{b}^{\mathrm{T}}\mathbf{M}\mathbf{b}$ as the Tikhonov-type VA-inspired stabilizer that controls weighted metrics properties of the image and its gradient flow map specified by the $K \times K$ matrix-form second-order pseudo differential operator $\mathbf{M} = \mathbf{I} + \nabla^2$ where $\mathbf{I}$ represents the discrete-form identity operator and $\nabla^2$ is the discrete-form spatial Laplacian defined via a 4-nearest-neighbors differences over the $x$-$y$ spatial coordinates in the scene frame [5, 18]). The ME-regularized solution on the minimum of (2) exists and is guaranteed to be unique because all functions that compose $E(\mathbf{b}|\boldsymbol{\lambda})$ are convex. Due to the nonlinearity of the composite error function (2), the derivation of the ME-regularized solution of the image restoration problem with system/method fusion requires extremely complex computations with proper collaborative adjustments of all "degrees of freedom" $\boldsymbol{\lambda}$ in (2) if solve this problem using the standard gradient descent-based minimization techniques, thus yields an NP hard computational problem [18, 19]. Our proposition is to solve that problem in a considerably speeded-up fashion using the MENN computational framework detailed in the next section.

## 4 MENN for RS System/Method Fusion

The multistate Hopfield-type dynamic MENN that we propose to employ to solve the fusion problem at hand is a $P$-mode expansion of the MENN developed in [11, 12] with the $K$-D state vector $\mathbf{x}$ and $K$-D output vector $\mathbf{z} = \mathrm{sgn}(\mathbf{W}\mathbf{x} + \boldsymbol{\theta})$, where $\mathbf{W}$ and $\boldsymbol{\theta}$ represent the matrix of synaptic weights and the vector of the corresponding bias inputs of the MENN, respectively, designed to aggregate all $P$ systems/methods to be fused. The state values $\{x_k; k = 1, \ldots, K\}$ of all $K$ neurons are used to represent the gray levels of the lexicographically ordered image vector in the process of the feature enhancing fusion. Each neuron $k$ receives the signals from all other neurons including itself and a bias input. The energy function of such a neural network (NN) is expressed as [11]

$$E = -\tfrac{1}{2}\mathbf{x}^{\mathrm{T}}\mathbf{W}\mathbf{x} - \boldsymbol{\theta}^{\mathrm{T}}\mathbf{x} = -\tfrac{1}{2}\sum_{k=1}^{K}\sum_{i=1}^{K} W_{ki}x_k x_i - \sum_{k=1}^{K}\theta_k x_k. \tag{3}$$

The idea for solving the RS system/method fusion problem using the MENN is based on the following proposition. If the energy function (3) of the NN represents the function of a mathematical minimization problem over a parameter space, then the state of the NN would represent the parameters and the stationary point of the network would represent a local minimum of the original minimization problem $\hat{\mathbf{b}} = \arg\min_{\mathbf{b}} E(\mathbf{b}|\boldsymbol{\lambda})$. Hence, utilizing the concept of a dynamic NN, we may translate our image recovery problem with RS system/method fusion to the correspondent

problem of minimization of the energy function (3) of the related MENN. Therefore, we define the parameters of the MENN to aggregate the corresponding parameters of all $P$ systems/methods to be fused adopting the equibalanced image ant its gradient map discrepancy $\ell_2$ squared norm [12] partial objective functions $\{J_p(\mathbf{b})\}$ in (2) that yields

$$W_{ki} = -\sum_{p=1}^{P}[\hat{\lambda}_p \sum_{j=1}^{K} \Phi_{jk}^{(p)} \Phi_{ji}^{(p)}] - \lambda_{P+1} M_{ki} \ , \tag{4}$$

$$\theta_k = -\ln b_k + \sum_{p=1}^{P}[\ \hat{\lambda}_p \sum_{j=1}^{K} \Phi_{jk}^{(p)} q_j^{(p)}\ ] \tag{5}$$

for all $k, i = 1, \ldots, K$. Next, to find a minimum of the energy function (3) with specifications (4), (5) the states of the network are to be updated $\mathbf{x}'' = \mathbf{x}' + \Delta\mathbf{x}$ (the superscripts $'$ and $''$ correspond to the state values before and after network state updating) to provide the non-positive energy changes

$$\Delta E \approx -(\sum_{i=1}^{K} W_{ki} x_i' + \theta_k' - 1)\Delta x_k - \tfrac{1}{2} W_{kk} (\Delta x_k)^2 . \tag{6}$$

due to updating of each $k$th neuron; $k = 1, \ldots, K$. To guarantee non-positive values of the energy changes (6) at each updating step the state update rule $\Re(\mathbf{z})$ should be as follows, $\Re(\mathbf{z})$: if $z_k = 0$, then $\Delta x_k = 0$; if $z_k > 0$, then $\Delta x_k = \Delta$; if $z_k < 0$, then $\Delta x_k = -\Delta$ for all $k = 1, \ldots, K$, where $\Delta$ is a prescribed step-size parameter. Following the original MENN prototype from [11, 12], we adopt $\Delta = 10^{-2}$ and the collaborative balancing method for empirical evaluation of the regularization parameters

$$\{\hat{\lambda}_p = \hat{q}^{-1}\hat{a}_p;\ \hat{a}_p = (\sum_{n=1}^{P} r_n)^{-1} r_p;\ \ p, n = 1, \ldots, P\} \tag{7}$$

directly from the degraded input images (1) where $r_p = \text{trace}\{(\mathbf{\Phi}^{(p)})^{-2}\}$ represents the $p$th system/method resolution factor [5], and the gain factor $\hat{q}$ is to be found as a solution to the so-called resolution-to-noise balance equation (Eq. (33) from [11]).

## 5 Simulation Results

To analyze the performances of different RS image formation techniques, we evaluated the effectiveness of the image formation and feature enhanced recovery via performing the computer simulations experiment. The test unfocused fractional SAR (F-SAR) system image was generated via performing the matched spatial filtering (MSF) [3, 4] of the high-resolution noised SAR 1024×1024-pixel scene image borrowed from the real-world RS imagery [20] with the squared triangular PSF of 10 pixel width in the range direction ($y$-axis) and the truncated squared Gaussian PSF of 30 pixel width in the azimuth direction ($x$-axis) to be comparable with the previous simulations formats [12, 16]. Different fusion combinations $\{p, p' \in P\}$ of two methods from the tested six ($P = 6$) specified in Table 1 were simulated and compared. For evaluation of the enhancement/fusion performances, we employed two metrics. The

first one is the conventional resolution enhancement over noise suppression measure referred to also as the signal-over-noise improvement (*SNI*) metric [17, 18]

$$SNI^{fused} = 10\log_{10}\frac{\sum_{k=1}^{K}\left(\frac{(g_k^{(p)}+g_k^{(p')})}{2}-b_k\right)^2}{\sum_{k=1}^{K}(\hat{b}_k^{fused}-b_k)^2} \tag{8}$$

where $b_k$ is the $k$th element of the test high-resolution image **b** of dimension $K$ = 1024×1024, $\{\hat{b}_k^{(p)}, \hat{b}_k^{(p')}\}$ represent the $k$th elements of the tested combinations $\{p, p' \in P = 6\}$ of the images fused in a particular simulation experiment, and $\{\hat{b}_k^{fused}\}$ represent the corresponding pixel values of the fused image for the particular tested combination $\{p, p' \in P = 6\}$. The second one is the mean absolute error [19]

$$MAE^{fused} = 10\log_{10}\left(\frac{1}{K}\sum_{k=1}^{K}\left|\frac{(g_k^{(p)}+g_k^{(p')})}{2}-b_k\right|\right);\ p, p' = 1,...,P \tag{9}$$

The quantitative method fusion results evaluated in both metrics (8), (9) are reported in Table 1, where subscripts $_1$ and $_2$ point at single-look and double-look F-SAR modalities: single-look (SNR = 0 dB) and double-look (SNR = 5 dB).



**Table 1.** *SNI* (8) and *MAE* (9) metrics corresponding to the reconstruction of the F-SAR image with five simulated fusion combinations (the modeled system parameters are the same as in the competing study[12]): range PSF width (at ½ from the peak value) $\kappa_r$ = 10 pixels; azimuth PSF width (at ½ from the peak value) $\kappa_a$ = 30 pixels; Indexes 1 and 2 point at two corresponding SNRs: $SNR_1$ = 0 dB (single look mode) and $SNR_2$ = 5 dB (double-look mode). The fusion was performed employing the MENN technique featured in Sect. 4 for the corresponding combinations of the DEDR-related techniques specified in Table 1. The dynamic MENN enhancement and fusion results are reported for 30 performed iterations for the VA-free DEDR-related techniques [11, 15] and for 8 iterations for the developed here DEDR-VA-MENN method.

| **Method Fusion Combination** | | | | | | |
|---|---|---|---|---|---|---|
| **Metric** | **$MSF_1$-$MSF_2$** | **$MSF_1$-$AD_2$** | **$MSF_1$-$RSF_2$** | **$MSF_1$-$RASF_2$** | **$MSF_1$-$APES_2$** | **DEDR-VA-MENN** |
| ***SNI* [dB]** | **7.92** | **8.39** | **8.73** | **9.17** | **9.74** | **10.79** |
| ***MAE* [dB]** | **20.17** | **19.34** | **17.43** | **15.34** | **13.16** | **12.38** |

In Fig. 1 we present the enhanced imaging results attained with different recovery techniques (as specified in the figure captions). The corresponding convergence rates for the three feasible combinations of the competing method fusion combinations are reported in Figure 2. Such $MSF_1$-$AD_2$, $MSF_1$-$RSF_2$ and DEDR-VA-MENN methods require 30.82, 38.51 and 10.46 seconds respectively, to converge when run in a PC at 3.4 GHz with an Intel Core i7 64-bit processor and 8.00 GB of RAM. Thus, our NN method is at least 3 times more efficient in comparison with the most competing ones.

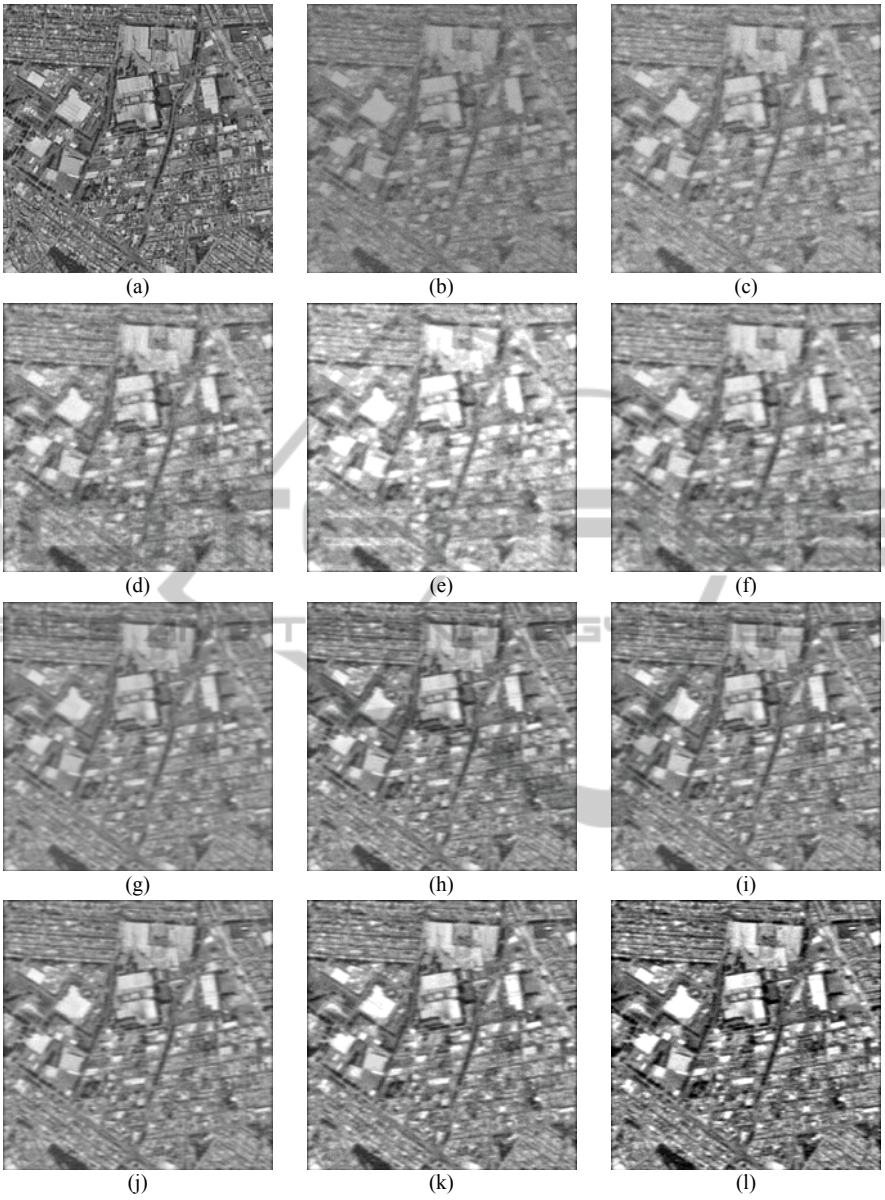


**Fig. 1.** Qualitative results of the F-SAR images enhancement without and with method fusion: (a) original 1024×1024-pixel scene from the real-world RS imagery [20]; (b) degraded F-SAR single look scene image; (c) AD enhancement (without fusion) [13], (d) RSF enhancement (without fusion) [16]; (e) RASF enhancement (without fusion) [17]; (f) APES enhancement (without fusion) [15]; (g) $MSF_1$-$MSF_2$ fusion; (h) $MSF_1$-$AD_2$ fusion; (i) $MSF_1$-$RSF_2$ fusion; (j) $MSF_1$-$RASF_2$ fusion; (k) $MSF_1$-$APES_2$ fusion; (l) DEDR-VA-MENN fusion. Subscripts $_1$ and $_2$ point at single-look mode ($SNR_1$ = 0 dB) and double-look ($SNR_2$ = 5 dB) F-SAR modalities. The VA-free enhanced imaging results (e)–(k) are reported for 30 performed iterations and the fused DEDR-VA-MENN enhancement result (l) is reported for 8 performed iterations.

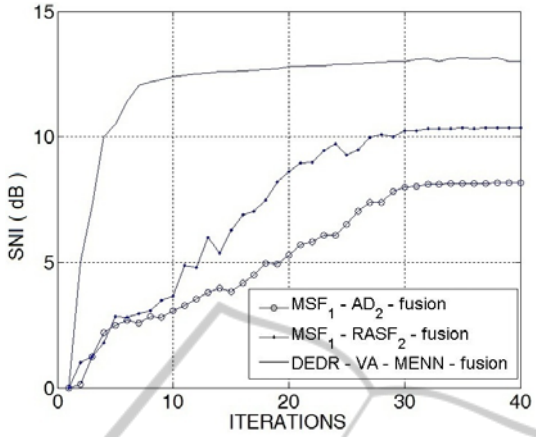


**Fig. 2.** Convergence rates evaluated via the *SNI* metric vs. number of iterations for three most prominent DEDR-related method fusion combinations (specified in the text box) implemented using the MENN computing technique featured in Sect. 4.



## 6 Conclusion

We have presented and validated via simulations a new approach for feature enhanced RS sensor/method fusion. In the heart of our method is adaptation of the MENN computational framework to solving the RS image fusion inverse problems. To achieve the feature enhanced fusion, we developed the technique for performing the aggregation of the DEDR and VA regularization paradigms that leads to proper adaptive adjustments of the MENN operational parameters (aggregated synaptic weights and bias inputs). The proposed aggregated DEDR-VA-MENN enhancement/fusion technique outperforms the existing low-resolution RS image formation approaches as well as the recently proposed competing robust adaptive RS image recovery methods that do not employ the multi-level structured regularization both in the resolution enhancement over noise suppression and convergence rates. These result in the speeded-up computational implementation with the considerably reduced (near-real) processing time. The reported simulations demonstrate and verify the feature enhanced recovery of the real-world RS imagery acquired with an F-SAR system operating in a harsh sensing environment.

## References

1. Curlander J.C., McDonough R.: Synthetic Aperture Radar—System and Signal Processing. Wiley, NY (1991)
2. Franceschetti G., Landari R.: Synthetic Aperture Radar Processing. Wiley, NY (2005)
3. Henderson F.M. A., Lewis V., Eds.: Principles and Applications of Imaging Radar, Manual of Remote Sensing, 3d ed., vol. 3, Willey, NY (1998)
4. Wehner D.R.: High-Resolution Radar, 2nd ed., Artech House, Boston, MA (1994)

5. Barrett H.H., Myers K.J.: Foundations of Image Science, Willey, NY (2004)
6. Lee J. S.: Speckle Suppression and Analysis for Synthetic Aperture Radar Images, Optical Engineering, vol. 25, no. 5, (1986) 636-643
7. Franceschetti G., Iodice A., Perna S., Riccio D.: Efficient Simulation of Airborne SAR Raw Data of Extended Scenes, vol. 44. No. 10. IEEE Trans. Geoscience and Remote Sensing (Oct. 2006) 2851-2860
8. Ishimary A.: Wave Propagation and Scattering in Random Media. IEEE Press, NY (1997)
9. Farina A.: Antenna-Based Signal Processing Techniques for Radar Systems, Artech House, Norwood, MA (1991)
10. Shkvarko Y.V.: Estimation of Wavefield Power Distribution in the Remotely Sensed Environment: Bayesian Maximum Entropy Approach, vol. 50, No. 9. IEEE Trans. Signal Proc. (Sep. 2002) 2333-2346,
11. Shkvarko Y.V., Shmaliy Y. S., Jaime-Rivas R. Torres-Cisneros M.: System Fusion in Passive Sensing Using a Modified Hopfield Network, vol. 338. Journal of the Franklin Institute (2000) 405–427
12. Shkvarko Y.V., Santos S.R., Tuxpan J.: Near Real-Time Enhancement of Fractional SAR Imagery via Adaptive Maximum Entropy Neural Network Computing, 2012 9th European Conference on Synthetic Aperture Radar (EUSAR'2012), ISBN: 978-3-8008-3404-7, Nurnberg, Germany (Apr. 2012) 792-795
13. Perona P. Malik J.: Scale-Space and Edge detection Using Anisotropic Diffusion, vol. 12. No. 7. IEEE Trans. Pattern Anal. Machine Intell. (July 1990) 629-639
14. Patel V.M., Easley G.R., Healy D.M., Chellappa R.: Compressed Synthetic Aperture Radar, vol. 4. No. 2. IEEE Journal of Selected Topics in Signal Proc. (2010) 244-254
15. Yarbidi T., J. Stoica Li, Xue P. M. Baggeroer A.B.: Source Localization and Sensing: A Nonparametric Iterative Adaptive Approach Based on Weighted Least Squares, vol. 46, No. 1. IEEE Trans. Aerospace and Electronic Syst. (2010) 425-443
16. Shkvarko Y.V., Tuxpan J., Santos S.R.: Dynamic Experiment Design Regularization Approach to Adaptive Imaging with Array Radar/SAR Sensor Systems, Sensors, no 5, (2011) 4483-4511
17. Shkvarko Y.V., Tuxpan J., Santos S.R.: High-Resolution Imaging with Uncertain Radar Measurement Data: A Doubly Regularized Compressive Sensing Experiment Design Approach, in Proc. IEEE 2012 IGARS Symposium, ISBN: 978-1-467311-51/12, Munich, Germany (July 2012) 6976-6970
18. Mathews J.H.: Numerical Methods for Mathematics, Science, and Engineering, Second Edition, Prentice Hall, Englewood Cliffs, NJ (1992)
19. Ponomaryov V., Rosales A., Gallegos F., Loboda I.: Adaptive Vector Directional filters to Process Multichannel Images, vol. E90-B, No. 2. IEICE Trans. Communications (Feb. 2007) 429–430
20. TERRAX-SAR Images, Available at: http://www.astrium-geo.com/en/19-galery?img=1690&search=gallery&type=0&sensor=26&resolution=0&continent=0&application=0&theme=0